

The scale of homogeneity in the local Universe with the ALFALFA catalogue

Felipe Avila,^a Camila P. Novaes,^a Armando Bernui,^a Edilson de Carvalho^{a,b}

^aObservatório Nacional,

Rua General José Cristino 77, São Cristóvão, 20921-400, Rio de Janeiro, RJ, Brazil

^bCentro de Estudos Superiores de Tabatinga, Universidade do Estado do Amazonas, 69640-000, Tabatinga, AM, Brazil

E-mail: felipeavila@on.br, camilapnovaes@gmail.com, bernui@on.br, edilsonfilho@on.br

Abstract. We use the scaled counts in spherical caps $\mathcal{N}(< \theta)$ and the fractal correlation dimension $\mathcal{D}_2(\theta)$ procedures to search for a transition scale to homogeneity in the local universe as given by the ALFALFA catalogue (a sample of extragalactic HI line sources, in the redshift range $0 < z < 0.06$). Our analyses, in the 2-dimensional sky projected data, show a transition to homogeneity at $\theta_H = 16.49^\circ \pm 0.29^\circ$, in remarkable accordance with the angular scale expected from simulations, a result that strengthens the validity of the cosmological principle in the local universe. We test the robustness of our results by analysing the data sample using three versions of the $\mathcal{N}(< \theta)$ estimator, which show a well agreement between them. These statistical estimators were validated using mock realizations generated assuming a fractal distribution of points, successfully recovering the input information. In addition, we perform further analyses showing that our approach is also able to indicate the presence of under- and over-densities in the data. Finally, we verify the influence of the sample size to the θ_H estimates by using segment Cox processes of different projected areas, confirming the suitability of the ALFALFA surveyed area for the current analyses.

Contents

1	Introduction	1
2	The Arecibo Legacy Fast ALFA Survey	2
3	Methodology	4
3.1	The scaled counts-in-spheres: the 3D case	4
3.2	The scaled counts-in-caps: the 2D case	5
3.2.1	Average, Centre, and Landy-Szalay estimators	5
3.3	The homogeneity scale criterium	6
4	Results	6
4.1	The angular scale of transition to homogeneity	6
4.2	Effects introduced by density fluctuations	7
4.2.1	Over-densities	8
4.2.2	Under-densities	9
4.3	Performance test with simulated fractal samples	9
4.4	Robustness tests with the segment Cox process	10
5	Conclusions	12

1 Introduction

The cosmological principle (CP) is at the basis of modern cosmology [1, 2]. The CP, together with Einstein’s equations, supports the concordance cosmological model, Λ CDM, which currently shows the best agreement with observational data (see, e.g., [3, 4] for a review of the concordance model and its key results). According to the CP, the Universe is expected to be homogeneous and isotropic at sufficiently large scales. With the advent of new and precise astronomical data, it becomes an open problem to estimate how large are these scales [5–7].

Nowadays, the study of the statistical isotropy of matter and radiation is an active research field. In the absence of information to know the cosmological distances, the *projected* isotropy [8], i.e., considering the sources projected on the sky, has been extensively tested with extra-galactic sources like X-ray [9], Radio [10, 11], Gamma-ray bursts [12–15], galaxy clusters [16] and full sky galaxy survey [17, 18], showing their compatibility with statistical isotropy. Besides, the *projected* isotropy of the Planck convergence map [19] and of the WISE galaxy map [20–23] have been also investigated without indications of a possible CP violation. The cosmic microwave background (CMB) radiation is also consistent with statistical isotropy at small angular scales [24–26], although some controversy exists at the largest scales [27–35].

The analysis of spatial homogeneity is more cumbersome. Methods that test the homogeneity of the matter distribution by counting objects in spheres or spherical caps (when the sources are projected on the sky) are not direct tests of spatial homogeneity. The information regarding the number of cosmic objects on spatial hyper-surfaces inside the past light-cone cannot be accessed by methods like *counts-in-spheres* because the counts are restricted to the intersection of the past light-cone with the spatial hyper-surfaces (see, e.g., [2, 5]). However, these methods provide consistency tests in the following sense: if the counts-in-spheres method shows that the objects distribution does not

approach homogeneity on large scales, then this can falsify the CP. Instead, if observations confirm the existence of a transition scale to homogeneity, then this strengthens the evidence for spatial homogeneity, but cannot prove it [2, 6].

The main difficulty to perform consistency tests concerns the low number density of cosmic objects achieved in past surveys, insufficient to obtain a good signal to noise ratio. Recent surveys, however, increased substantially the volume of the observed universe and the purity of the cosmic tracers samples, promoting this type of analysis.

The counts-in-spheres method is being widely used to explore the homogeneity scale in diverse cosmological tracers. It is based on the idea that, for a homogeneous sample, when averaging the normalized number of cosmic objects inside spheres of radius r , $N(< r)$, one should observe a behaviour like $N(< r) \propto r^3$ when increasing the sphere radius r as large as possible. This estimator gives a relatively good measure for real surveys with peculiar geometry, but its correlation matrix reveals that their measurements are highly correlated. Alternatively, one can use the *fractal correlation dimension*, $\mathcal{D}_2(r)$, which has the advantage to be essentially uncorrelated between bins of distance [8, 36, 37], besides to correct some systematic effects like holes or gaps in the survey geometry, the catalogue incompleteness, and needs not to assume homogeneity at large scales as required in the correlation function estimator [39].

Applying the scaled counts-in-spheres and the fractal correlation dimension procedures in 3-dimensional (3D) analyses, it was recently reported the transition scale to homogeneity for blue galaxies from the WiggleZ survey, with redshifts $0.1 < z < 0.9$ [36]. More recently it was also applied to galaxy catalogues [37, 40] and to quasars sample [8, 38, 41, 42] of the Sloan Digital Sky Survey (SDSS). In addition, it was used to confirm that the transition scale varies as a function of the universe age [37, 43]: the higher the redshift the less clumpy is the matter. However, despite the robustness of these studies, they used the standard cosmological model to calculate distances which, in some way, may bias the results. With this in mind, some authors [43–45] worked on an independent model analysis, studying the homogeneity with projected 2D data.

In this work we search for the angular scale of transition to homogeneity in the 2D sky projected data using the ALFALFA catalogue. The ALFALFA project is a radio survey that observed extragalactic HI line sources of the local universe, $0 < z < 0.06$. We use these extraordinary data to explore the homogeneity scale in the local universe because the recently released catalogue is 100% complete and has a very good ratio between surveyed area and detected number of objects [46, 47] (for other applications of this dataset see, e.g., [48, 49]).

This work is organized as follows. In section 2 we present briefly some features of the survey. In section 3 we describe the method of scaled counts-in-spheres and its definitions. In sections 4 and 5 we show our results and present our conclusions, respectively.

2 The Arecibo Legacy Fast ALFA Survey

The Arecibo Legacy Fast ALFA Survey¹ (ALFALFA) is a catalogue of extragalactic HI line sources, in 21 cm, which cover an area of $\sim 7000 \text{ deg}^2$. Most of the sources detected are gas-rich galaxies with low surface brightness and dwarfs that populate the local universe $0 < z < 0.06$ [47, 50]. Recently, it has been released the first version of the full ALFALFA catalogue², with 100% of the footprint area, containing 33573 objects classified in three categories according to its HI

¹<http://egg.astro.cornell.edu/alfalfa/data/index.php>

²The catalogue analysed here was kindly provided by M. P. Haynes, on behalf of the ALFALFA collaboration, before the public release.

line detection status: CODE 1, high signal to noise ratio extragalactic sources, considered highly reliable and with confirmed optical counterpart; CODE 2, lower signal to noise ratio HI signal coincident with optical counterpart, considered unreliable sources; and CODE 9, high signal to noise ratio source with no optical counterpart and likely Galactic high velocity cloud. In this work we shall use only the sources designated as CODE 1, as recommended by the ALFALFA team. The ALFALFA survey covers two continuous regions, both in the declination range $0^\circ < \text{DEC} < 36^\circ$, in the right ascensions intervals of $21^{\text{h}}30^{\text{m}} < \text{RA} < 3^{\text{h}}15^{\text{m}}$ and $7^{\text{h}}20^{\text{m}} < \text{RA} < 16^{\text{h}}40^{\text{m}}$. The first region, referred as *Fall sky*, contains a total of 11433 HI sources and the second one, the *Spring sky*, have 22140 HI sources.

Here we consider only the Spring sky region, illustrated in the left panel of figure 1, which encompasses a larger number of sources. Moreover, to minimize possible effects introduced by the irregularity of the survey geometry, we restrict the analyses to the region defined by the coordinates $9^{\text{h}}20^{\text{m}} \leq \text{RA} \leq 15^{\text{h}}50^{\text{m}}$ and $0^\circ \leq \text{DEC} \leq 36^\circ$, as illustrated in the right panel of figure 1. The final sample has 13144 HI sources of CODE 1, whose redshift distribution is shown in figure 2.

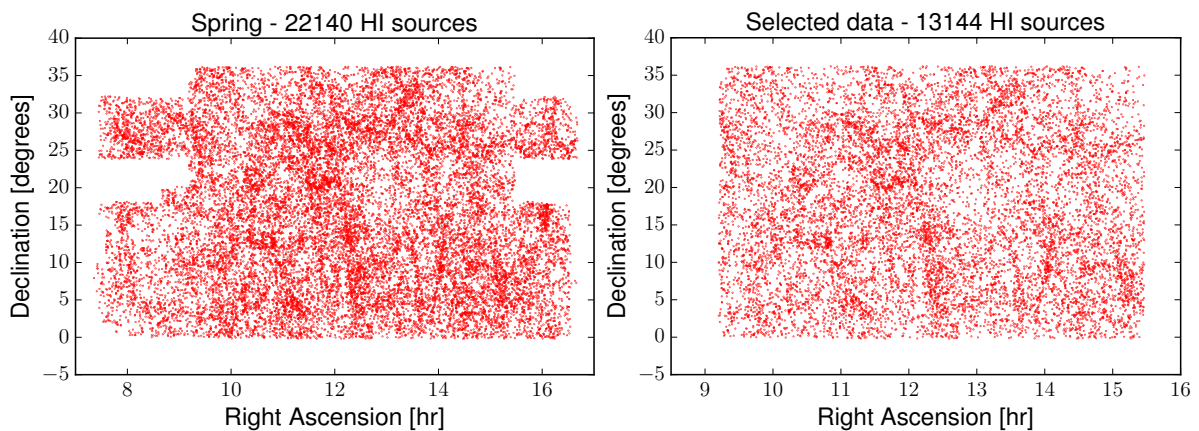


Figure 1. **Left:** Cartesian projection of the area corresponding to the Spring sky region. **Right:** Cartesian projection of the final selected sample for analyses. Note the cuts in RA on the left and right sides of the Spring sky to minimize possible systematics introduced by the irregular geometry of the survey.

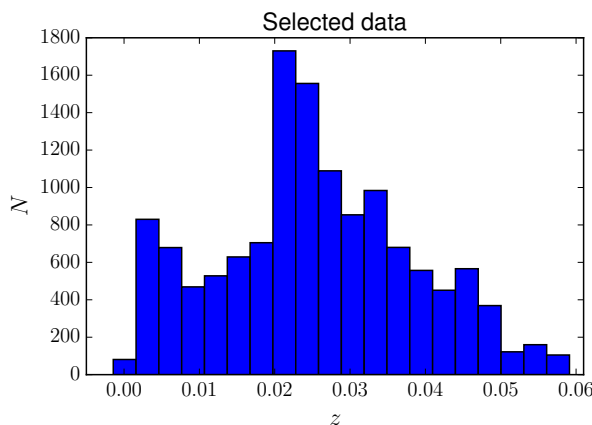


Figure 2. Redshift distribution of sources in the final sample selected from the ALFALFA catalogue (corresponding to the right panel of figure 1).

3 Methodology

This section describes the methodology adopted for our homogeneity analyses. We present the scaled counts-in-spheres method, $\mathcal{N}(< r)$, and the equivalent quantity adapted to the 2D analyses we consider here, the scaled counts-in-caps (or spherical caps), $\mathcal{N}(< \theta)$, calculated through three different estimators, besides the related fractal correlation dimension, \mathcal{D}_2 . Finally, we describe how they can be adapted to analyse the ALFALFA dataset, in addition to our criterium to determine the transition scale to homogeneity, θ_H .

3.1 The scaled counts-in-spheres: the 3D case

To study the homogeneity of a dataset it is commonly adopted the counts-in-spheres estimator, $N(< r)$, which does not depend on hypotheses like homogeneity and completeness of the analysed sample. This quantity corresponds to the average number of objects encompassed by a sphere of a radius r , with $r_{\min} \leq r \leq r_{\max}$, centred around each object of the catalogue. Clearly, the choices for the values r_{\min} and r_{\max} to perform the numerical analyses depend on the features of the catalogue in scrutiny. For a 3D homogeneous distribution of objects one expects that

$$N(< r) \propto r^3. \quad (3.1)$$

For the general case of a fractal distribution of objects we have [51]

$$N(< r) \propto r^{D_2}, \quad (3.2)$$

where D_2 is termed the fractal correlation dimension (or just correlation dimension), defined as

$$D_2(r) \equiv \frac{d \ln N(< r)}{d \ln r}. \quad (3.3)$$

However, it is not feasible to use this equation directly estimated from $N(< r)$, since the results can be biased by the survey geometry (in special, the boundary effects) and incompleteness of the sample [8]. Aiming to reduce these effects it is introduced the estimator termed scaled counts-in-spheres, $\mathcal{N}(< r)$, defined as [36]

$$\mathcal{N}(< r) \equiv \frac{N_{gal}(< r)}{N_{rand}(< r)}, \quad (3.4)$$

where $N_{gal}(< r)$ is the average counting estimated for spheres centred at each source of the data catalogue and $N_{rand}(< r)$ is the same quantity calculated upon a random homogeneous sample, using as centres the coordinate positions of the data catalogue sources. Then, the correlation dimension in terms of $\mathcal{N}(< r)$ is written as

$$\mathcal{D}_2(r) \equiv \frac{d \ln \mathcal{N}(< r)}{d \ln r} + 3. \quad (3.5)$$

As discussed in section 3.4 of ref. [8], for the scientific objective of our analyses, the estimator \mathcal{D}_2 is a more suitable estimator because, differently of $\mathcal{N}(< r)$, it is essentially uncorrelated between r bins.

3.2 The scaled counts-in-caps: the 2D case

In this work we analyse the ALFALFA data projected on the sky, which requires the spheres of radius r mentioned above, for the 3D case, to be replaced by spherical caps of angular radius θ , so that Equation (3.5) must be accordingly modified. As detailed in ref. [43], the $\mathcal{D}_2(r)$ estimator adapted to the 2D projection of the data sample on the sphere \mathcal{S}^2 , $\mathcal{D}_2(\theta)$, is given by

$$\mathcal{D}_2(\theta) = \frac{d \ln \mathcal{N}(< \theta)}{d \ln \theta} + \frac{\theta \sin \theta}{1 - \cos \theta}, \quad (3.6)$$

where the counts-in-caps (or spherical caps) is given by

$$\mathcal{N}(< \theta) \equiv \frac{N_{gal}(< \theta)}{N_{rand}(< \theta)}. \quad (3.7)$$

Note from Equation (3.6) that for a homogeneous angular distribution one has: $\mathcal{D}_2(\theta) \rightarrow \theta \sin \theta / (1 - \cos \theta)$, for sufficiently large θ value.

3.2.1 Average, Centre, and Landy-Szalay estimators

The literature provides some estimators for the \mathcal{N} quantity (see, e.g., ref. [43]). Here we employ three of them, namely, the *Average estimator*

$$\mathcal{N}_j^A(< \theta) \equiv \frac{\frac{1}{n_g} \sum_{i=1}^{n_g} N_{gal}^i(< \theta)}{\frac{1}{n_g} \sum_{i=1}^{n_g} N_{rand}^{i,j}(< \theta)}, \quad (3.8)$$

the *Centre estimator*

$$\mathcal{N}_j^C(< \theta) \equiv \frac{1}{n_g} \sum_{i=1}^{n_g} \frac{N_{gal}^i(< \theta)}{N_{rand}^{i,j}(< \theta)}, \quad (3.9)$$

where n_g is the number of objects in the data sample, and the third estimator, that is based on the Landy-Szalay (LS) two-point angular correlation function [52, 53],

$$\omega_j^{LS}(\theta) = \frac{DD(\theta) - 2DR(\theta) + RR(\theta)}{RR(\theta)}, \quad (3.10)$$

and for this called *LS estimator*

$$\mathcal{N}_j^{LS}(< \theta) \equiv 1 + \frac{1}{1 - \cos \theta} \int_0^\theta \omega_j^{LS}(\theta') \sin \theta' d\theta', \quad (3.11)$$

calculated for the j th random catalogue. $DD(\theta)$ is defined as the number of pairs of galaxies in the data sample, for a given θ , normalized to the total number of pairs; $RR(\theta)$ is the same quantity calculated for the random catalogue; and $DR(\theta)$ corresponds to the number of pairs between the data and random catalogues, normalized to the total number of pairs in the data and random catalogues.

Then, we use Equation 3.6 to obtain the corresponding $\mathcal{D}_2^j(\theta)$ data points, for the j th random catalogue, in the range $1^\circ \leq \theta \leq 40^\circ$ and bins of $\Delta\theta = 1^\circ$. For this work we constructed 20 random homogeneous catalogues with the same geometry and number n_g of objects as the ALFALFA catalogue. Therefore, the final $\mathcal{D}_2(\theta)$ quantity is then estimated from the arithmetic mean: $\mathcal{D}_2(\theta) = (1/20) \sum_{j=1}^{20} \mathcal{D}_2^j(\theta)$, for each of the three estimators. Notice that the integral in Equation 3.11 is calculated over the best-fit curve of the $\omega_j^{LS}(\theta)$ data points, previously estimated using Equation 3.10 (see, e.g., [8, 37]).

3.3 The homogeneity scale criterium

First we fit a model-independent polynomial to the $\mathcal{D}_2(\theta)$ data points calculated as described in previous sections. Then, to determine the scale of transition to homogeneity, θ_H , we consider the 1%-criterium commonly adopted in the literature [8, 36, 37, 43]: we identify the scale at which the fitted curve reach 99% of the \mathcal{D}_2^H threshold value expected for a homogeneous distribution. For the case of a 2D (3D) Euclidean space this value is a constant, $\mathcal{D}_2^H = 2$ ($\mathcal{D}_2^H = 3$), while for a distribution on the 2D celestial sphere S^2 it is a function of θ [43],

$$\mathcal{D}_2^H(\theta) \equiv \frac{\theta \sin\theta}{1 - \cos\theta}. \quad (3.12)$$

Thus, the value θ_H is the scale where

$$\mathcal{D}_2(\theta_H) = 0.99 \mathcal{D}_2^H(\theta_H). \quad (3.13)$$

Despite the 1%-criterium is arbitrary, it has positive attributes to have been widely adopted in the literature (for a complete discussion about the positive and negative attributes of several criteria see [36]); perhaps the most useful feature is its independence with the data sample in study, allowing an easy comparison among different analyses.

4 Results

In this section, we present in detail the results we obtain applying the three estimators, *Average*, *Centre*, and *LS*, to the ALFALFA catalogue. We also evaluate the effects that density fluctuations, given by structures like *voids* and galaxy clusters, i.e. under- and over-densities, can introduce in the \mathcal{D}_2 and, consequently, in the estimates of the angular scale of transition to homogeneity. These analyses are specially important when the surveyed volume coverage is suitable to encompass such type of structures in the local universe, as is the case of the ALFALFA catalogue. We also perform consistency tests of the estimators, by using fractal catalogues, to verify if the use of $\mathcal{N}(< \theta)$ is biasing our results. Additionally, we generate and analyse realizations of segment Cox processes to confirm the suitability of the ALFALFA area for the current analyses.

4.1 The angular scale of transition to homogeneity

The median redshift of the final sample selected from the ALFALFA catalogue is $z_m \simeq 0.025$, for this we refer to it as a representative of the local universe. Our main results analysing this dataset can be seen in figure 2, for the *Average* and *Centre* estimators, and in the left panel of figure 4, for the *LS* estimator. As can be observed, the three estimators are in good agreement in the determination of the homogeneity angular scale, θ_H , obtaining a value around 16° . In each case, this scale is measured through a polynomial fit for the \mathcal{D}_2 data points calculated for each of the 20 random catalogues individually (gray curves). We used a polynomial of order three in the case of the *Average* and *Centre* estimators, with an average *root mean square error*³ of $E = 0.0064$ and 0.0078 , respectively, and of order five for the *LS* estimator, with $E = 0.0012$. In the estimates showed in table 1, the error bars correspond to the 68% confidence level obtained from a *bootstrap resampling* of the 20 values of θ_H estimated using each of the random catalogues.

³The degree of the polynomial is chosen to be the one minimizing E , taking into account the Akaike Information Criterion to penalize the number of free parameters of the fit.

From the analyses presented in refs [44, 45], performed using simulated catalogues generated with bias $b = 1$ and redshift ranges of thickness comparable to ours, we extrapolate the θ_H estimated there to the redshift range we are considering, obtaining 32.46° for the expected value of the homogeneity scale. However, according to ref. [55], extragalactic HI line sources have an anti-bias b with respect to the matter fluctuations ($b = 1$), namely, a factor that varies between $0.48 - 0.68$, depending on the richness of the sample. Therefore, the expected value for the homogeneity scale, for the specific case of the data we are analysing, is estimated to be $15.58^\circ \lesssim \theta_H \lesssim 22.07^\circ$ (table 1).

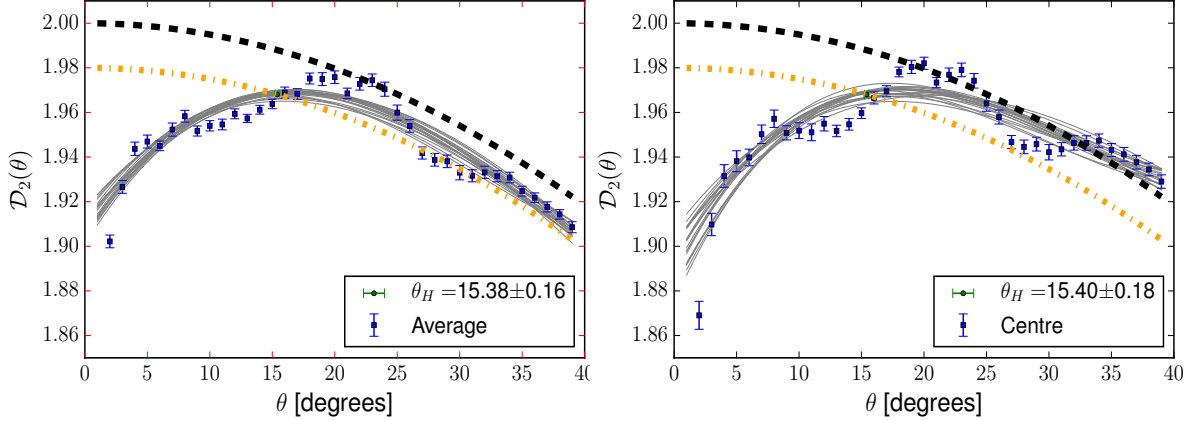


Figure 3. **Left:** $\mathcal{D}_2(\theta)$ data points (blue dots) obtained from Equation 3.6 for the *Average* estimator (Equation 3.8) in the range $1^\circ \leq \theta \leq 40^\circ$, with bins size $\Delta\theta = 1^\circ$. The corresponding error bars were obtained from the standard deviation from the 20 random catalogues. The black dashed line represents the threshold value for $\mathcal{D}_2(\theta)$ when the distribution is considered homogeneous, i.e., the $\mathcal{D}_2^H(\theta)$ curve given by Equation 3.12. The orange dot-dashed line represents the 1% below this threshold (the 1%-criterion given by Equation 3.13). The gray curves correspond to polynomial fits of order three for the $\mathcal{D}_2(\theta)$ points measured using each one of the 20 random catalogues, whose intersection with the orange dot-dashed line determines the angular scale of transition to homogeneity, θ_H . The green dot is the mean over these 20 values and its error bar is obtained using the bootstrap method (see subsection 4.1 for details). **Right:** Similar to the information displayed in the left panel, but now the data analysis was done with the *Centre* estimator (Equation 3.9).

	<i>Average</i> estimator	<i>Centre</i> estimator	<i>LS</i> estimator	expected [44, 45]
θ_H	$15.38^\circ \pm 0.16^\circ$	$15.40^\circ \pm 0.18^\circ$	$16.49^\circ \pm 0.29^\circ$	$[15.58^\circ, 22.07^\circ]$

Table 1. In this table we summarize our findings, that is, the angular scale of transition to homogeneity as measured by our three estimators. We also show, in the last column, the value expected according to simulations, done for matter fluctuations ($b = 1$) [44, 45], that we extrapolated to our sample considering the ALFALFA redshift range and the appropriate bias factor [55].

4.2 Effects introduced by density fluctuations

First of all, it is worth to notice the features clearly appearing in the $\mathcal{D}_2(\theta)$ curves obtained from the *Average* and *Centre* estimators (figure 3), presenting successive data points below and above the $\mathcal{D}_2^H(\theta)$ threshold expected for a homogeneous distribution (black dashed line given by Equation 3.12). This is still confirmed by a similar behaviour of the ω^{LS} data points around the best-fit curves

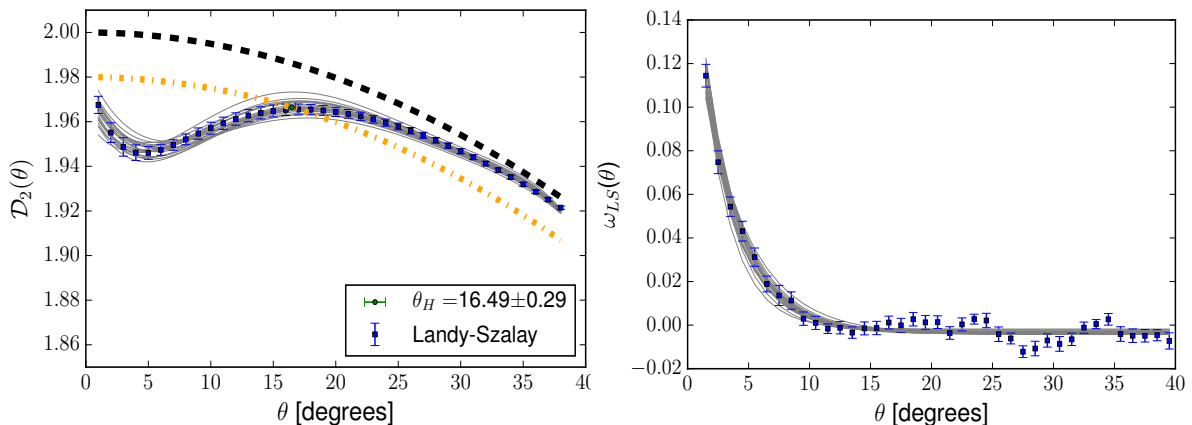


Figure 4. **Left:** Similar to the information displayed in figure 3 but for the analyses done with the *LS* estimator (Equation 3.11). **Right:** Average of the *LS* two-point angular correlation function, ω_{LS}^{LS} , calculated through Equation 3.10, for the 20 random catalogues, $\omega^{LS} = \langle \omega_j^{LS} \rangle$, for $j = 1, \dots, 20$ (blue dots). The error bars correspond to the 1σ dispersion over these 20 estimates. The gray curves are the best-fit of the ω_j^{LS} data points, used to calculate $\mathcal{D}_2^j(\theta)$ for the j th random catalogue (see section 3.2.1 for details).

(gray lines) in the right of figure 4, a signature likely associated to density fluctuations on the sample⁴. Such behaviour seems not only to indicate the presence of under- or over-dense regions in the data sample, but also, and more interestingly, to furnish information about the extension and how under- or over-dense could be such regions. Specifically, one can identify features appearing in the scale intervals of $\sim 8^\circ - 16^\circ$ (this one only in the *Average* and *Centre* \mathcal{D}_2) and $\sim 25^\circ - 33^\circ$, which could be associated to under-densities, while the one in scale range $\sim 20^\circ - 25^\circ$ seems to be influenced by the presence of an over-density. Therefore, below we present results of additional analyses performed not only to verify these statements, but also to evaluate how under- and over-densities appearing in the data sample can affect our analyses.

4.2.1 Over-densities

In this section we investigate in detail the possible presence of an over-dense region suggested by the fact that the $\mathcal{D}_2(\theta)$ data points overtake the threshold curve $\mathcal{D}_2^H(\theta)$ (given by the black dashed line in figure 3; see also Equation 3.12). To elucidate if a clustering of objects in a small region can produce this effect we first identify the candidate objects, remove them from the catalogue in study, and then repeat our analyses. The objects we chose to remove belong to the Virgo cluster, a known structure appearing in the data sample we analyse. In the principal reference of the ALFALFA survey [50], the objects belonging to the Virgo cluster are identified as mainly standing at distances between 16 – 18 Mpc. Moreover, we use the recent catalogue of sources belonging to the Virgo cluster to identify the angular region encompassing most of them, namely, $0^\circ \leq \text{DEC} \leq 20^\circ$ and $12^{\text{h}} \leq \text{RA} \leq 13^{\text{h}}30^{\text{m}}$ [54]. For illustrative purposes, in the left panel of figure 5 we highlight with a different color the objects belonging to this region, from where it is visually noticeable that they appear clustered. Finally, using the *Average* estimator we show at the right panel of figure 5 a comparison among the analyses of the ALFALFA sample with and without the presence of the Virgo cluster. One can clearly observe from this graph that without these objects the $\mathcal{D}_2(\theta)$ data points remain below the threshold curve; with

⁴Notice that these features do not appear in the \mathcal{D}_2 obtained with the *LS* estimator because we use the best-fit curve over the ω_j^{LS} data points to estimate $\mathcal{N}_j^{LS}(< \theta)$, from which we obtain the corresponding \mathcal{D}_2^j and mean \mathcal{D}_2 .

a similar behaviour from the *Centre* estimator. Moreover, notice that the difference between the two analyses, with and without this structure, is restricted to scales around $\theta \sim 20^\circ$, indicating a possible relation with the cluster dimension. Therefore, this confirms our preliminary suspicion that, indeed, the Virgo cluster is an over-density that manifests itself by overtaking the \mathcal{D}_2^H curve at the scale $20^\circ - 25^\circ$.

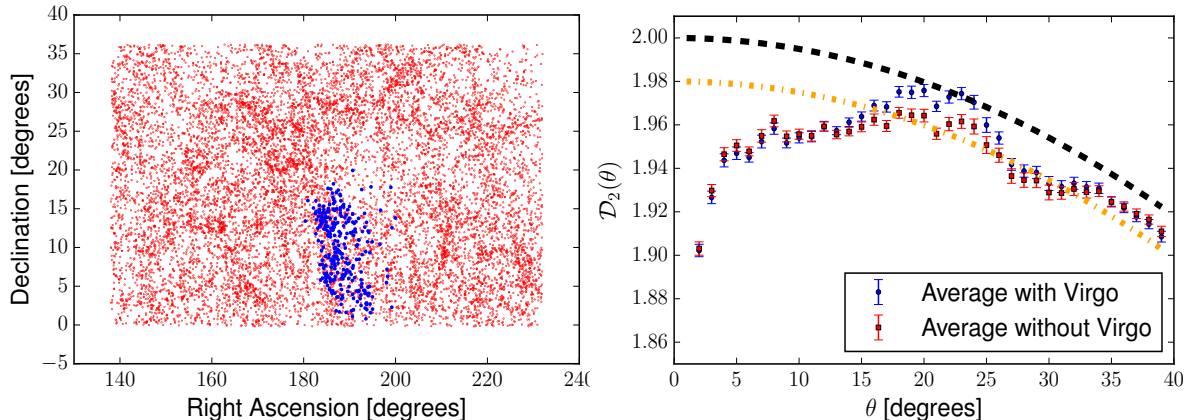


Figure 5. **Left:** Plot of the selected ALFALFA sample highlighting in blue color the 287 objects in between $16 - 18$ Mpc in distance, $0^\circ \leq \text{DEC} \leq 20^\circ$ in declination, and $12^{\text{h}} \leq \text{RA} \leq 13^{\text{h}}30^{\text{m}}$ in right ascension, possibly belonging to the Virgo cluster. **Right:** For comparison, we show the $\mathcal{D}_2(\theta)$ estimates obtained with the *Average* estimator when analysing the data sample with and without the objects highlighted in blue in the left panel, i.e., the Virgo cluster. Again the black dashed and orange dot-dashed line represent, respectively, the \mathcal{D}_2^H threshold for a homogeneous sample (Equation 3.12) and the 1% below it, given by Equation 3.13.

4.2.2 Under-densities

As mentioned above, our $\mathcal{D}_2(\theta)$ analyses suggest the presence of under-densities at the scale intervals $8^\circ - 16^\circ$ and $25^\circ - 33^\circ$. In order to verify this, we perform a test analogous to the one in the previous section, but removing (masking) the under-dense region, a disk of radius 5° at $\text{RA} = 13^{\text{h}}$ (193°) and $\text{DEC} = 17.5^\circ$ (left panel of figure 6). Such area was identified by using a void-finder like code, which perform a scan in the whole projected data sample looking for the region of lowest number density.

The right panel of figure 6 shows the $\mathcal{D}_2(\theta)$ data points obtained by applying the *Average* estimator to the masked ALFALFA sample (red squares), where we also include the results from the non-masked sample (blue dots). From the comparison among them we conclude that, as expected, the presence of under-dense regions in the sample tends to decrease the $\mathcal{D}_2(\theta)$ values corresponding to the size of that regions. This can be seen from the amplitude of these data points around $8^\circ - 16^\circ$, which increases when excluding the under-dense region from the analysis, the opposite behaviour to that observed when we removed the Virgo members. Therefore, this confirms our expectation that the presence of both, over- and under-densities, have a definite influence in the behaviour of the $\mathcal{D}_2(\theta)$ function and impact the scale transition to homogeneity.

4.3 Performance test with simulated fractal samples

In this section we use fractal realizations, constructed according to a predefined \mathcal{D}_2 value, to look for possible bias introduced in $\mathcal{N}(< r)$ by the methodology considered here, in special, due to boundary effects. For this test we consider 100 realizations, with a mean of ~ 22000 points distributed on the same geometry as the selected ALFALFA data but on a 2D Euclidean plane \mathcal{R}^2 . Then we

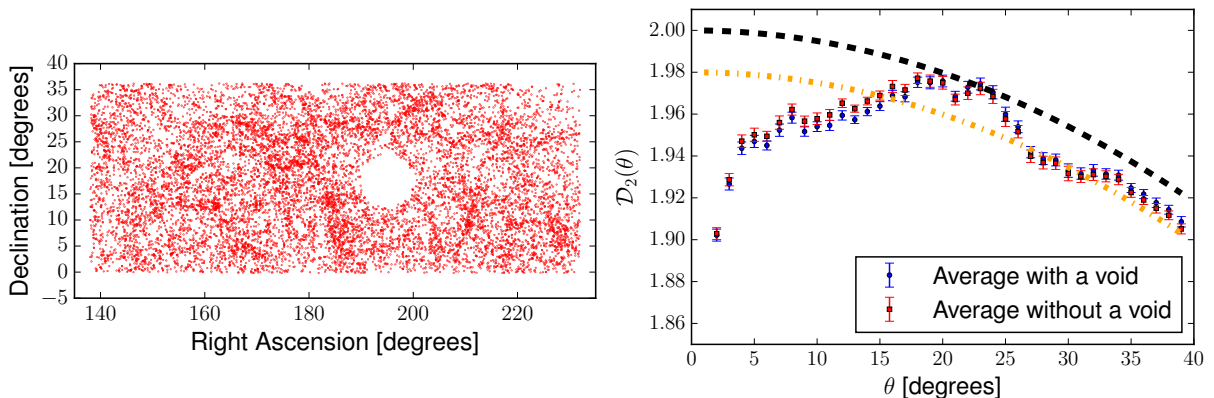


Figure 6. **Left:** ALFALFA sample after removing an under-dense area. The masked region correspond to a circle of 5° radius (i.e., an object of size 10°) centred at RA, DEC = $(193^\circ, 17.5^\circ)$. **Right:** $\mathcal{D}_2(\theta)$ estimated applying the *Average* estimator to the ALFALFA sample before (blue dots) and after (red squares) masking an under-dense area.

compute $\mathcal{N}(< r)$ and $\mathcal{D}_2(r)$ using disks, where distances r (in arbitrary units) are calculated with the Euclidean geometry.

Each realization is a self-similar fractal sample generated using a modified β -model [51]. First, consider a square of side L , and divide it in $M = n^2$ squares of side L/n . Then, impose a survival probability p to each square at each iteration, and repeat this process k times. In the limit of infinite iterations we would have

$$D_2 = \lim_{k \rightarrow \infty} \frac{\log(pM)^k}{\log n^k} = \frac{\log(pM)}{\log n}. \quad (4.1)$$

The value of D_2 defines the probability p through the Equation 4.1. For our purposes to construct realizations with fractal dimension $D_2 = 1.9$, it is enough to perform $k = 7$ iterations in order to get a sample with approximately the same number of points as objects in the selected data. What we expect to recover in this analysis is therefore $D_2 \simeq 1.9$, for large distances.

We applied the *Average* and *Centre* estimators to the 100 fractal realizations, using 10 random homogeneous catalogues in each evaluation of D_2 . The random catalogues were produced considering homogeneously distributed data in the same geometry and with the mean number of points as each of the 100 fractal samples (strictly speaking, since the number of points can vary from one fractal sample to another, different samples require random catalogues with different number of points). Our results can be seen in figure 7, where we satisfactorily recover the input fractal dimension, obtaining the mean values $\bar{D}_2 = 1.91818$ for the *Average* estimator and $\bar{D}_2 = 1.91824$ for the *Centre* estimator. The error bars are the standard deviation from the 100 realizations. We also test for others fractal dimensions, namely 1.8 and 1.85, recovering values close to the input ones.

4.4 Robustness tests with the segment Cox process

Additionally to the previous tests, performed to evaluate the robustness of our results and enhance our comprehension of the features observed, this section presents one additional test whose aim is to evaluate the influence of the observational constraint considering the size of the area selected with ALFALFA data. For this, we use the *segment Cox point process*, i.e., artificial catalogues generated given a characteristic length scale l [56, 57]. Such samples are generated by randomly placing segments of length l in a box of side L , with a mean number of segments per unit volume λ_s , i.e., a length density of segments $L_V = \lambda_s l$, and then randomly distributing points on these segments.

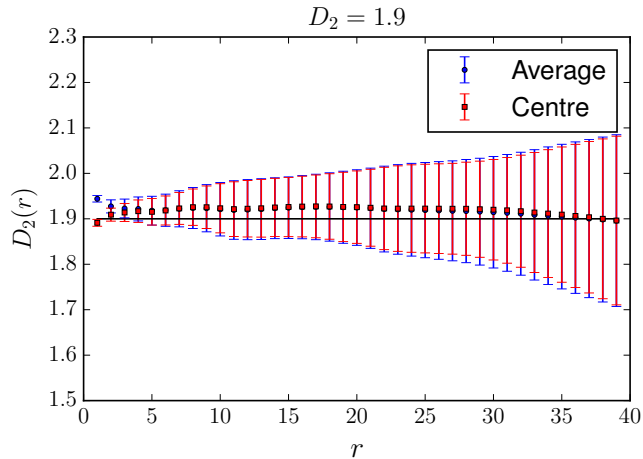


Figure 7. Average $\mathcal{D}_2(r)$ estimated from 100 fractal realizations, generated with an approximate number of points as objects in the ALFALFA catalogue and distributed in the same geometry as in the left panel of figure 6. The error bars represent the 1σ deviation from these samples. The black line corresponds to the input $\mathcal{D}_2 = 1.9$ value.

The intensity of the point process, i.e., the number density of points in the volume, is given by $\lambda = \lambda_l L_V = \lambda_l \lambda_s l$, where λ_l is the average number of points per unit length of a segment.

We generate 20 segment Cox processes for different values of l , namely, $l = 10$ and 20 Mpc, fixing $\lambda_l = 1$ and varying λ_s in such a way to achieve a number density close to the ALFALFA projected sample. These samples were constructed considering a box of volume 2.16×10^8 Mpc³, where the observer is at the center. In this way the projection of the simulated catalogue results in a distribution of objects in the whole 2D sphere, so that we are free to take a region of any area needed. We construct and analyse segment Cox processes of two projected areas: A , which is the area of the ALFALFA sample, and $2A$, twice its area; the second one corresponds to the region delimited by the coordinates $0^\circ \leq \text{DEC} \leq 72^\circ$ and $138^\circ \leq \text{RA} \leq 232^\circ$. Before projecting the sample, we randomly shift the points by using a Gaussian distribution of $\sigma = 0.5$ [58], smearing out the strong clustering of the segments, which helps to diminish the noise in the resulting \mathcal{D}_2 . An example of a segment Cox process is exhibited in the left panel of figure 8.

Each one of the 20 segment Cox processes, for given l (10 or 20 Mpc) and area (A or $2A$), was analysed following the same procedure used to analyse the ALFALFA data sample, as well as the 1% criterium to determine the transition scale. Moreover, each sample was analysed using the same 20 random catalogues used previously (section 4.1), i.e., one has 20 values of θ_H for each simulated catalogue, leading to a total of $20 \times 20 = 400$ values of θ_H for given l and area. Table 2 summarizes the results obtained from the *Average* estimator, presenting in the third and fifth columns the mean and standard deviation of each set of 400 values, for the cases where the area is equal to A and $2A$, respectively. It is evident the very good agreement between the θ_H estimates analysing different areas, within their error bars, showing smaller values for $2A$ due to the better statistics for a larger area.

A comparison among the results from different areas can also be seen from the right panel of figure 8, showing the general behaviour of the \mathcal{D}_2 points averaged over 20 segment Cox processes constructed with $l = 20$ Mpc for A (red dots) and $2A$ (blue squares). One observes in this plot the same asymptotic behaviour and equal transition scale to homogeneity, in both cases using the 1% criterium. Therefore, the analyses of different segment Cox processes let us to conclude that the projected area of the ALFALFA sample is suitable for the analyses we perform here.

l [Mpc]	λ_s^A	θ_H^A	λ_s^{2A}	θ_H^{2A}
10	2.31×10^{-4}	$9.79^\circ \pm 0.63^\circ$	2.78×10^{-4}	$9.38^\circ \pm 0.37^\circ$
20	1.48×10^{-4}	$11.13^\circ \pm 1.33^\circ$	1.16×10^{-4}	$10.62^\circ \pm 0.61^\circ$

Table 2. Results from applying the *Average* estimator to segment Cox processes for two different l values, 10 and 20 Mpc, and two projected areas, A and $2A$. The displayed θ_H values and error bars correspond to the mean and one standard deviation of the total of 400 values estimated from the 20 simulations of each type (20 θ_H values for each simulation; see the text for details). In all the cases we used $\lambda_l = 1.0$.

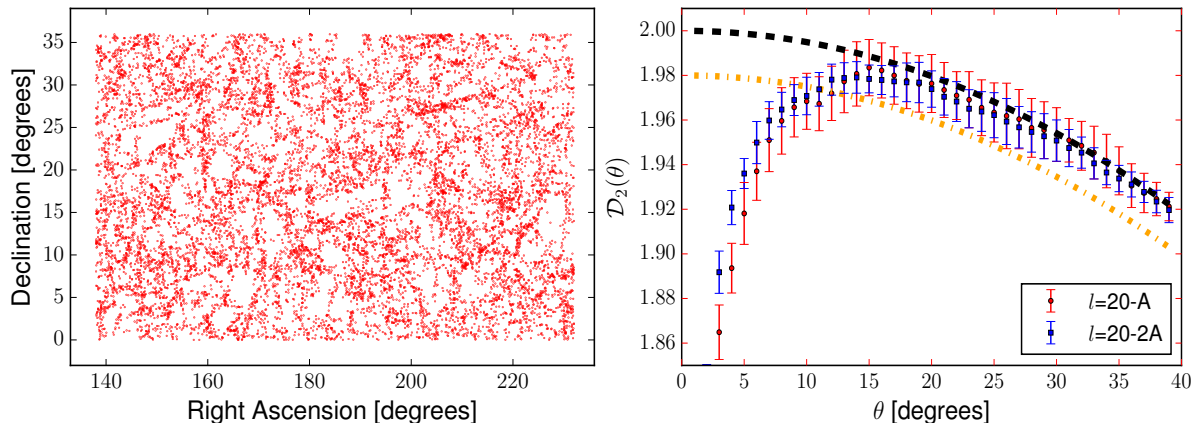


Figure 8. **Left:** Illustrative example of a segment Cox process for $l = 20$, with the same number density of objects and projected area A of the ALFALFA sample, after performing a Gaussian shift of the data positions with $\sigma = 0.5$. **Right:** Correlation dimension $\mathcal{D}_2(\theta)$ averaged over 20 segment Cox processes constructed with $l = 20$ Mpc on the area A (red dots) and other 20 on area $2A$ (blue squares). The error bars correspond to one standard deviation of the data from these simulations. These analyses were done using the *Average* estimator.

5 Conclusions

The recent progress in surveying tracers of the large scale structure has substantially increased the volume of the observed universe. This facility has allowed the exploration of the CP, in special the analyses of the homogeneity of the Universe, which require a high density of cosmic objects. Although we are not capable to prove its validity, one can still perform consistency tests of such property. In this work we used the scaled counts-in-caps and the fractal correlation dimension to measure the angular scale corresponding to the transition to homogeneity in the local universe ($0 < z < 0.06$), using the recently released ALFALFA catalogue. The methodology adopted, besides it has been extensively employed in the literature, exhibits the advantage that it does not rely on the geometric details or incompleteness of the data survey.

Our angular scale analyses, in the 2D sky projected data from ALFALFA, reveal a transition to homogeneity that appears robust because: (i) we have performed analyses considering three estimators obtaining, basically, the same transition scale (see section 4); (ii) interesting features appearing at several scales in the $D_2(\theta)$ data points, are –after detailed analyses– associated with under- and over-densities present in the dataset (see sections 4.2 and 4.2.2); (iii) our procedures were successfully tested with simulated catalogues, including fractal realizations (see section 4.3) and segment Cox processes (see section 4.4).

Regarding the use of three estimators, it is worth to mention that one estimator can reveal aspects

that other estimator ignores, for this the convenience of appreciate the features revealed by diverse estimators. In fact, as observed in section 4, the *Average* and *Centre* estimators reveal the presence of under- and over-dense regions through features appearing in the $D_2(\theta)$ data points, while the *LS* estimator expose them directly in the 2-point correlation functions, ω^{LS} . And with respect to possible observational effects due to matter clustering or voidness in the survey, the way we analyse them is with the aid of simulations that help us to verify their plausible presence through the signatures they leave in the estimators, even when they are not so large neither visually observed in the surveyed area. As a consequence of such detailed analyses, we show that clusters and voids can affect the measurement of the transition scale to homogeneity. Additionally, we also investigate if the size of the projected 2D area of the ALFALFA selected sample can influence the measurement of the transition scale to homogeneity, θ_H . By applying the *Average* estimator to segment Cox processes of different projected areas, one with the same area of the ALFALFA and the other with twice its area, we achieved results consistent one with each other within their 1σ error bars (see Table 2 and figure 8). This confirms the suitability of the ALFALFA surveyed area for the current analyses.

Other interesting issues regard observational systematics, like instrumental effects, masks, possible contaminations, survey geometry, etc., which can be source of errors or uncertainties. For this, the ALFALFA team made efforts to correct or minimize them, resulting in a dataset of excellent quality detection in HI, objects termed as CODE 1, considered here in our analyses. In addition, in the current release the survey is 100% complete and has a very good ratio between surveyed area and detected number of objects.

Our main result is presented in table 1. There we show the estimate obtained for the angular scale of transition to homogeneity, $\theta_H \simeq 16^\circ$, when analysing the local universe data given by the 2D projection of the final selected sample of the ALFALFA catalogue (see section 2). This estimate is in agreement with the value expected according to simulations assuming a fiducial Λ CDM cosmology [44, 45]. For this we confirm the existence of an angular scale of transition to homogeneity, a result that strengths the CP.

Acknowledgments

FA, CPN, and AB acknowledge fellowships from CAPES, FAPERJ, and CNPq, respectively. EdC acknowledges the PROPG-CAPES/FAPEAM program. We would like to thank Joel Carvalho, Rodrigo S. Gonçalves, Jailson Alcaniz, and Roy Maartens for useful comments and productive feedback of our analyses. We acknowledge M. P. Haynes and the ALFALFA team for the use of the data.

References

- [1] J.A. Peacock, *Cosmological Physics*, Cambridge University Press, Cambridge U. K. (1999).
- [2] R. Maartens, *Is the Universe homogeneous?*, *Phil. Trans. Roy. Soc.* **A369** (2011) 5115 [arXiv:1104.1300]
- [3] J. Lesgourgues, *An overview of Cosmology*, (2004) [arXiv:0409426]
- [4] W.J. Percival, *Large Scale Structure Observations*, (2013) [arXiv:1312.5490]
- [5] C. Clarkson, *Establishing homogeneity of the Universe in the shadow of dark energy*, *C. R. Phys.* **13** (2012) 682 [arXiv:1204.5505]
- [6] A. Heavens, R. Jimenez, R. Maartens, *Testing homogeneity with the fossil record of galaxies*, *JCAP* **09** (2011) 035 [arXiv:1107.5910]

- [7] W. Valkenburg, V. Marra, C. Clarkson, *Testing the Copernican principle by constraining spatial homogeneity*, *Mon. Not. Roy. Astron. Soc.* **438** (2014) L6 [arXiv:1209.4078]
- [8] P. Laurent, et al., *A $14h^{-3}Gpc^3$ study of cosmic homogeneity using BOSS DR12 quasar sample*, *JCAP* **11** (2016) 060 [arXiv:1602.09010]
- [9] C.A. Scharf, et al., *The 2-10 keV X-ray background dipole and its cosmological implications*, *Astrophys. J.* **544** (2000) 49 [arXiv:9908187]
- [10] C. Blake, J. Wall, *A velocity dipole in the distribution of radio galaxies*, *Nature* **416** (2002) 150 [arXiv:0203385]
- [11] S. Ghosh, et al., *Probing Statistical Isotropy of Cosmological Radio Sources using Square Kilometre Array*, *J. Astrophys. Astron.* **37** (2016) 25 [arXiv:1610.08176]
- [12] A. Bernui, I.S. Ferreira, C.A. Wuensche, *On the large-scale angular distribution of short-Gamma ray bursts*, *Astrophys. J.* **673** (2008) 968 [arXiv:0710.1695]
- [13] J. Řípa, A. Shafiello, *Testing the Isotropic Universe Using the Gamma-Ray Burst Data of Fermi/GBM*, *Astrophys. J.* **851** (2017) 15 [arXiv:1706.03556]
- [14] M. Tarnopolski, *Testing the anisotropy in the angular distribution of Fermi/GBM gamma-ray bursts*, *Mon. Not. Roy. Astron. Soc.*, **472** (2017) 4819 [arXiv:1512.02865]
- [15] J. Ripa, A. Shafieloo, *Update on Testing Isotropic Universe Using Properties of Gamma-Ray Bursts*, (2018) [arXiv:1809.03973]
- [16] C.A.P. Bengaly, A. Bernui, J.S. Alcaniz, I.S. Ferreira, *Probing cosmological isotropy with Planck Sunyaev-Zeldovich galaxy clusters*, *Mon. Not. Roy. Astron. Soc.* **466** (2017) 2799 [arXiv:1511.09414]
- [17] B. Pandey, *Testing isotropy in the Two Micron All-Sky redshift survey with information entropy*, *Mon. Not. Roy. Astron. Soc.* **468** (2017) 1953 [arXiv:1703.01184]
- [18] R.S. Menezes, C. Pigozzo, S. Carneiro, *Testing cosmic isotropy with galaxies position angles distribution*, (2017) [arXiv:1705.02323]
- [19] G.A. Marques, C.P. Novaes, A. Bernui, I.S. Ferreira, *Isotropy analyses of the Planck convergence map*, *Mon. Not. Roy. Astron. Soc.* **473** (2018) 165 [arXiv:1708.09793]
- [20] C.A.P. Bengaly, A. Bernui, J.S. Alcaniz, H.S. Xavier, C.P. Novaes, *Is there evidence for anomalous dipole anisotropy in the large-scale structure?*, *Mon. Not. Roy. Astron. Soc.* **464** (2017) 768 [arXiv:1606.06751]
- [21] M. Yoon, D. Huterer, C. Gibelyou, A. Kovács, I. Szapudi, *Dipolar modulation in number counts of WISE-2MASS sources*, *Mon. Not. Roy. Astron. Soc.* **445** (2014) L60 [arXiv:1406.1187]
- [22] C.A.P. Bengaly, et al., *The dipole anisotropy of WISExSuperCOSMOS number counts*, *Mon. Not. Roy. Astron. Soc.* **475** (2018) L106 [arXiv:1707.08091]
- [23] C.P. Novaes, et al., *Tomographic local 2D analyses of the WISExSuperCOSMOS all-sky galaxy catalogue*, *Mon. Not. Roy. Astron. Soc.* **478** (2018) 3253 [arXiv:1805.04078]
- [24] Planck Collaboration, *Planck 2013 results. XXIII. Isotropy and statistics of the CMB*, *Astron. Astrophys.* **571** (2014) A23 [arXiv:1303.5083]
- [25] Planck Collaboration, *Planck 2015 results. XVI. Isotropy and statistics of the CMB*, *Astron. Astrophys.* **594** (2016) A16 [arXiv:1506.07135]
- [26] C.P. Novaes, A. Bernui, G.A. Marques, I.S. Ferreira, *Local analyses of Planck maps with Minkowski Functionals*, *Mon. Not. Roy. Astron. Soc.* **461** (2016) 1363 [arXiv:1606.04075]
- [27] A. Bernui, *Is the cold spot responsible for the CMB North-South asymmetry?*, *Phys. Rev. D* **80** (2009) 123010 [arXiv:0912.1147]
- [28] L.R. Abramo et al., *Searching for planar signatures in WMAP*, *JCAP* **12** (2009) 013 [arXiv:0909.5395]

- [29] A. Gruppuso, et al., *Low variance at large scales of WMAP 9 year data*, *JCAP* **07** (2013) 047 [arXiv:1304.5493]
- [30] L. Polastri, A. Gruppuso, P. Natoli, *CMB low multipole alignments in the Λ CDM and dipolar models*, *JCAP* **04** (2015) 018 [arXiv:1503.01611]
- [31] D.J. Schwarz, C.J. Copi, D. Huterer, G.D. Starkman, *CMB anomalies after Planck*, *Class. Quantum Grav.* **33** (2016) 184001 [arXiv:1510.07929]
- [32] A. Bernui, A.F. Oliveira, T.S. Pereira, *North-South non-Gaussian asymmetry in PLANCK CMB maps*, *JCAP* **10** (2014) 041 [arXiv:1404.2936]
- [33] P.K. Aluri, J.P. Ralston, A. Weltman, *Alignments of parity even/odd-only multipoles in CMB*, *Mon. Not. Roy. Astron. Soc.* **472** (2017) 2410 [arXiv:1703.07070]
- [34] P.K. Rath, P.K. Samal, S. Panda, D.D. Mishra, P.K. Aluri, *Testing statistical Isotropy in Cosmic Microwave Background Polarization maps*, *Mon. Not. Roy. Astron. Soc.* **475** (2017) 4357 [arXiv:1707.04076]
- [35] A. Bernui, C.P. Novaes, T.S. Pereira, G.D. Starkman, *Topology and the suppression of CMB large-angle correlations*, (2018) [arXiv:1809.05924]
- [36] M.I. Scrimgeour, et al., *The WiggleZ Dark Energy Survey: the transition to large-scale cosmic homogeneity*, *Mon. Not. Roy. Astron. Soc.* **425** (2012) 116 [arXiv:1205.6812]
- [37] P. Ntelis, et al., *Exploring cosmic homogeneity with the BOSS DR12 galaxy sample*, *JCAP* **06** (2017) 019 [arXiv:1702.02159]
- [38] P. Ntelis, et al., *The scale of cosmic homogeneity as a standard ruler*, (2018) [arXiv:1810.09362]
- [39] P.H. Coleman, L. Pietronero, *The fractal structure of the Universe*, *Phys. Rep.* **213** (1992) 311
- [40] P. Sarkar, S. Majumdar, B. Pandey, A. Kedia, S. Sarkar, *The many scales to cosmic homogeneity: Use of multiple tracers from the SDSS*, (2016) [arXiv:1611.07915]
- [41] S. Nadathur, *Seeing patterns in noise: gigaparsec-scale ‘structures’ that do not violate homogeneity*, *Mon. Not. Roy. Astron. Soc.* **434** (2013) 398 [arXiv:1306.1700]
- [42] R. S. Gonçalves, et al., *Measuring the scale of cosmic homogeneity with SDSS-IV DR14 quasars*, *Mon. Not. Roy. Astron. Soc.* **481** (2018) 5270 [arXiv:1809.11125]
- [43] R.S. Gonçalves, et al., *Cosmic homogeneity: a spectroscopic and model-independent measurement*, *Mon. Not. Roy. Astron. Soc.* **475** (2018) L20 [arXiv:1710.02496]
- [44] D. Alonso, A. Bueno Belloso, F.J. Sánchez, J. García-Bellido, E. Sánchez, *Measuring the transition to homogeneity with photometric redshift surveys*, *Mon. Not. Roy. Astron. Soc.* **440** (2014) 10 [arXiv:1312.0861]
- [45] D. Alonso, A.I. Salvador, F.J. Sánchez, M. Bilicki, J. García-Bellido, E. Sánchez, *Homogeneity and isotropy in the Two Micron All Sky Survey Photometric Redshift catalogue*, *Mon. Not. Roy. Astron. Soc.* **449** (2015) 670 [arXiv:1412.5151]
- [46] R. Giovanelli, M.P. Haynes, *Extragalactic HI surveys*, *Astron. Astrophys. Rev.* **24** (2015) 1 [arXiv:1510.04660]
- [47] M.P. Haynes, et al., *The Arecibo Legacy Fast ALFA Survey: The ALFALFA Extragalactic HI Source Catalog*, *Astrophys. J.* **861** (2018) 49 [arXiv:1805.11499]
- [48] Y. Zu, *HI gas content of SDSS galaxies revealed by ALFALFA: implications for the mass-metallicity relation and the environmental dependence of HI in the local Universe*, (2018) [arXiv:1808.10501v2] [submitted].
- [49] M.G. Jones, M.P. Haynes, R. Giovanelli, C. Moorman, *The ALFALFA HI mass function: a dichotomy in the low-mass slope and a locally suppressed ‘knee’ mass*, *Mon. Not. Roy. Astron. Soc.* **477** (2018) 2 [arXiv:1802.00053]

- [50] M.P. Haynes, et al., *The Arecibo Legacy Fast ALFA Survey: the α .40 HI source catalog, its characteristics and their impact on the derivation of the HI mass function*, *Astron. J.* **142** (2011) 170 [arXiv:1109.0027]
- [51] C. Castagnoli, A. Provenzale, *From small-scale fractality to large-scale homogeneity-A family of cascading models for the distribution of galaxies*, *Astron. Astrophys.* **246** (1991) 634
- [52] S.D. Landy, A.S. Szalay, *Bias and variance of angular correlation functions*, *Astrophys. J.* **412** (1993) 64
- [53] E. de Carvalho, et al., *Angular Baryon Acoustic Oscillation measure at $z=2.225$ from the SDSS quasar survey*, *JCAP* **04** (2018) 064 [arXiv:1709.00113]
- [54] S. Kim, et al., *The Extended Virgo Cluster Catalog*, *The Astrophys. J. Suppl.* **215** (2014) 22 [arXiv:1409.3283]
- [55] S. Basilakos, M. Plionis, K. Kovač, N. Voglis, *Large-scale structure in the HI Parkes All-Sky Survey: filling the voids with HI galaxies?*, *Mon. Roy. Astron. Soc.* **378** (2007) 301 [arXiv:0703713]
- [56] V. J. Martínez, et al., *Searching for the scale of homogeneity*, *Mon. Roy. Astron. Soc.* **298** (1998) 1212 [arXiv:9804073]
- [57] M. J. Pons-Bordería, et al., *Comparing estimators of the galaxy correlation function*, *The Astrophys. J.* **523** (1999) 480 [arXiv:9906344]
- [58] V. Martínez, E. Saar, *Clustering statistics in cosmology*, *Proceedings of SPIE* **4847** (2002) 86 [arXiv:0209208]
- [59] B. Pandey, *Statistically significant length-scale of filaments as a robust measure of galaxy distribution*, *Mon. Not. Roy. Astron. Soc.* **468** (2010) 2687 [arXiv:0910.0711]